



# Persistent neuroinflammation and behavioural deficits after single mild traumatic brain injury

Antoine Drieu<sup>1</sup>, Anastasia Lanquetin<sup>1</sup>, Paul Prunotto<sup>1</sup>, Zuhul Gulhan<sup>2</sup>, Swannie Pédrón<sup>1</sup>, Gloria Vegliante<sup>3</sup>, Daniele Tolomeo<sup>3</sup>, Sophie Serrière<sup>2</sup>, Johnny Vercouillie<sup>2</sup>, Laurent Galineau<sup>2</sup>, Clovis Tauber<sup>2</sup>, Bertrand Kuhnast<sup>4</sup>, Marina Rubio<sup>1</sup>, Elisa R Zanier<sup>3</sup>, Damien Levard<sup>1</sup> , Sylvie Chalon<sup>2</sup>, Denis Vivien<sup>1,5</sup> and Carine Ali<sup>1</sup>

## Abstract

Despite an apparently silent imaging, some patients with mild traumatic brain injury (TBI) experience cognitive dysfunctions, which may persist chronically. Brain changes responsible for these dysfunctions are unclear and commonly overlooked. It is thus crucial to increase our understanding of the mechanisms linking the initial event to the functional deficits, and to provide objective evidence of brain tissue alterations underpinning these deficits. We first set up a murine model of closed-head controlled cortical impact, which provoked persistent cognitive and sensorimotor deficits, despite no evidence of brain contusion or bleeding on MRI, thus recapitulating features of mild TBI. Molecular MRI for P-selectin, a key adhesion molecule, detected no sign of cerebrovascular inflammation after mild TBI, as confirmed by immunostainings. By contrast, *in vivo* PET imaging with the TSPO ligand [<sup>18</sup>F]DPA-714 demonstrated persisting signs of neuroinflammation in the ipsilateral cortex and hippocampus after mild TBI. Interestingly, immunohistochemical analyses confirmed these spatio-temporal profiles, showing a robust parenchymal astrogliosis and microgliosis, at least up to 3 weeks post-injury in both the cortex and hippocampus. In conclusion, we show that even one single mild TBI induces long-term behavioural deficits, associated with a persistent neuro-inflammatory status that can be detected by PET imaging.

## Keywords

Mild traumatic brain injury, molecular MRI, neuroinflammation, persisting behavioural deficits, TSPO microPET imaging

Received 4 January 2022; Revised 17 June 2022; Accepted 20 June 2022

## Introduction

Each year, 69 million people suffer a traumatic brain injury (TBI), which is the leading cause of mortality in young adults and a major cause of death and disability across all ages worldwide.<sup>1,2</sup> The classification of TBI can be etiological, symptomatologic, prognostic or anatomopathological. Practice guidelines include structural imaging and neurological scoring, including the 15-point Glasgow Coma Scale, in their criteria for classifying injury severity as being severe, moderate, or mild TBI.<sup>3</sup> Clinical research has mainly been directed toward moderate and severe TBI, but the majority (70–90%) of patients suffer from mild TBI (miTBI).

<sup>1</sup>Normandie Univ, UNICAEN, INSERM, INSERM UMR-S U1237, Physiopathology and Imaging of Neurological Disorders, Institut Blood and Brain @ Caen-Normandie, Cyceron, France

<sup>2</sup>UMR 1253, iBrain, Université de Tours, INSERM, Tours, France

<sup>3</sup>Department of Neuroscience, Istituto di Ricerca Farmacologica Mario Negri, IRCCS, Milan, Italy

<sup>4</sup>IMIV, Service Hospitalier Frédéric Joliot, CEA, Inserm, Université Paris Sud, CNRS, Université Paris-Saclay, Orsay, France

<sup>5</sup>Department of Clinical Research, Caen-Normandie Hospital (CHU), Caen, France

## Corresponding author:

Carine Ali, INSERM U1237, GIP Cyceron, boulevard Becquerel, 14074 Caen, France.

Email: ali@cyceron.fr

Cumulative epidemiological data show that moderate or severe TBI, and very likely mild TBI, are important risk factors for disabilities (the so-called “silent epidemic”), including neurodegenerative diseases or psychiatric disorders.<sup>4–6</sup> The sparse quantitative estimations vary greatly, but patients with mild TBI may suffer from physical symptoms, cognitive dysfunctions, anxiety, depression, post-traumatic stress disorder, that risk to interfere with professional or social life.<sup>1,7,8</sup> Mild TBI is thus a serious condition and it is important to predict who are at risk patients and to understand the underlying pathogenic mechanisms. The current armamentarium remains insufficient, but imaging, or multimodal imaging is likely a key to success for these goals.

After the initial biomechanical injury, TBI induces a progressive secondary injury, which includes a neuroinflammatory response.<sup>9</sup> Accordingly, the ability to monitor inflammatory responses can have major diagnostic/prognostic implications for TBI. Beside plasma/CSF biomarkers, some brain biomarkers of inflammation can be targeted in humans by molecular imaging such as single photon emission computed tomography (SPECT) or positron emission tomography (PET). In this context, highly sensitive imaging of neuroinflammation is available using translocator protein (TSPO) PET ligands. Indeed, brain imaging of TSPO is now recognized as a relevant index of active microglia and is increasingly used in acute brain injuries such as stroke<sup>10</sup> neurodegenerative diseases such as Alzheimer’s disease and multiple sclerosis,<sup>11,12</sup> and moderate to severe TBI.<sup>13</sup> In parallel, molecular magnetic resonance imaging (MRI) to study endothelial activation has recently emerged as a promising axis of research,<sup>14</sup> with solid proof-of-concept studies in animal models. The recently developed contrast agents called micro-sized particles of iron oxide (MPIO) have significantly improved molecular MRI sensitivity and specificity. MPIOs harboring antibodies against adhesion molecules recruited at the endothelial luminal membrane (including VCAM-1 and P-selectin), have proven as highly relevant MRI tools to detect neuroinflammation in various pathological conditions,<sup>15–17</sup> including transient ischemic attack for which –like for miTBI –conventional MRI shows no evidence of brain infarction.<sup>18</sup>

Here, in mice, we tailored a model of miTBI below any detectable damage by conventional MRI, to test whether miTBI is associated to selective cognitive deficits and whether advanced translatable imaging of inflammation by molecular MRI or PET may inform on functional post-TBI sequelae.

## Material and methods

### Ethics

All experiments were performed and reported in accordance with the Animal Research: Reporting of In Vivo Experiments (ARRIVE) guidelines (<http://www.nc3rs.org.uk><sup>19</sup>) in accordance with French laws (act no. 87–848; Ministère de l’Agriculture et de la Forêt), European Communities Council Directives of November 24, 1986 (86/609/EEC) guidelines, and have been approved by the ethical committee (authorization number #15301). The Mario Negri Institute adheres to the principles set out in the following laws, regulations, and policies governing the care and use of laboratory animals: Italian Governing Law (D.lgs 26/2014; Authorization no.19/2008-A issued March 6, 2008 by Ministry of Health). They were reviewed and approved by the Mario Negri Institute Animal Care and Use Committee which includes ad hoc members for ethical issues, and by the Italian Ministry of Health (Decreto no. D/07/2013-B and 301/2017-PR).

### Animals

Experiments were performed on two months-old male Swiss mice (35–45 g; Centre Universitaire de Ressources Biologiques, Normandy University, Caen, France) or on male C57BL/6J mice (20–24 g; from Envigo for the Istituto di Ricerche Farmacologiche Mario Negri). Animals were housed at 21°C in a 12 h light/dark cycle with food and water with *ad libitum* free access. For each experiment, the number of animals used has been approved by the ethical committee. Sample sizes have been defined via an online power analysis tool (<https://clincalc.com/stats/samplesize.aspx>) and/or on our expertise.

### Surgical procedure for traumatic brain injury

For surgeries, mice were anesthetized with isoflurane 5% and maintained under anesthesia with 1.5–2.5% isoflurane in a 70%/30% gas mixture (N<sub>2</sub>O/O<sub>2</sub>). The body temperature was maintained at 37 ± 0.5°C throughout using a feedback-regulated heating system. Breathing was constantly checked and adjusted with anesthesia level. A sagittal incision (not midline to avoid major bleeding) was made to expose the skull. Mice were placed on a stereotaxic frame, and the head was maintained using both nose and ear bars. The whole body was elevated using a 3 cm-high box to limit contrecoup injuries. Then, the left parietal skull was cleaned with a cotton bud. Close-head controlled cortical impact (CCI) brain injury was induced using a 3 mm diameter rigid impactor driven by an electromagnetic controlled impact device (ImpactOne, Leica<sup>20</sup>)

rigidly mounted at an angle of 20° from the vertical plane and applied between the bregma and lambda of the left exposed skull (deformation depth was either 1.5 mm for mild TBI (miTBI) and 2 mm for moderate TBI (modTBI); velocity: 5.0 m/s; time of impact: 0.2 s, see schematic cartoon in Fig. S1). Using these two depths, skull fractures were not detected in miTBI mice, but were present on modTBI mice. Mice were sutured and placed in a separate box until recovery (i.e., restoration of a normal gait). Sham animals were subjected to the same procedure, except that they did not receive any impact.

As positive controls of molecular imaging, a series of mice was either injected with LPS in the striatum (1 µg) or subjected to severe TBI, induced by a 1 mm depth impact after craniectomy, as described earlier.<sup>21</sup>

### MRI of brain lesions

Mice were deeply anesthetized with 5% isoflurane in 30/70% O<sub>2</sub>/N<sub>2</sub>O and then maintained under anesthesia during all the experiment with 1.5–2.5% anesthesia in 30/70% O<sub>2</sub>/N<sub>2</sub>O. Imaging was carried out on a Pharmascan 7T/12 cm system using surface coils (Bruker, Germany). T2-weighted sequences were used to visualize oedema formation at 1, 7 and 21 days post-TBI using MSME sequences (multi-spin multi-echo): TE/TR: 51 ms/2500 ms TE/TR 33 ms/2500 ms with a 70\*70\*500 µm<sup>3</sup> spatial resolution. Haemorrhagic events were assessed using T2\*-weighted sequences (TE/TR: 7.7 ms/500 ms TE/TR 8.7064 ms/500 ms). Lesion size was calculated using Image J software (v1.52k, NIH).

### Behavioural assessments

A separate group of animals was subjected to behavioural tests before and after inducing mild or moderate TBI. Based on the literature,<sup>22,23</sup> our minimally invasive sham procedure was not expected to impact the behavioural parameters measured *per se*, so that no sham animals were included. Mouse weight was monitored before each behavioural assessment, the day and the day after the surgical procedure. A control MRI (T2 and T2\*) session was systematically performed 24 h after surgery to exclude animals with lesion and/or bleeding. One mouse with moderate TBI died a few days after surgery and two mice displayed brain haemorrhage after mild TBI; these three animals have thus been excluded from further analyses.

**Place recognition test.** Spatial memory was tested 7 days before and 7 and 21 days after mild TBI (n = 10 mice/group) in a white plastic Y-maze with three identical arms (34 × 7 × 14.5 cm). Mice were tested after a

two-session procedure with a 2h30 intersession interval, as previously described.<sup>24</sup> During the acquisition session, one arm was randomly closed with a guillotine door. The position of the closed arm was chosen randomly among the three arms. Each mouse was placed in one of the two other arms (arms A and B, with its head facing away from the center of the maze) and allowed to explore the two accessible arms for 5 min. Mice were then placed in their home cage for 2h30 before being subjected to the retention test, in which they had free access to all three arms for 5 min. The number of visits to each arm (considered only when the mouse passed two-thirds of the arm) was recorded for each session. Spatial memory was assessed through the comparison of the percentage of visits in each arm for the 5 min of the retention test. In the absence of deficits, the percentage of visits in the new arm is higher than 33% (the threshold of random visit).

**Open field.** Mice were placed in a squared box (31.5 × 31.5 cm) for 10 minutes as previously described,<sup>25</sup> 7 days before and 7 and 21 days after mild TBI (n = 10 mice/group). Animals were video-tracked (DMK 21AF04, The Imaging Source®) and distance and velocity were analyzed with EthoVision XT 11.5 software (Noldus). Additionally, a central region of 15 × 15 cm was defined, and the percentage of time spent in the center area was measured to assess anxiety-like behaviour. Rodents typically spend more time exploring the periphery of the arena by walking along the walls (thigmotaxis) than the central area.<sup>26</sup>

### Targeting-moiety conjugation to MPIOs and molecular imaging

Microparticles of iron oxide (MPIOs; diameter 1.08 µm) with p-toluenesulphonyl reactive surface groups (Invitrogen) were used for peptide conjugation.<sup>16</sup> Purified polyclonal goat anti-mouse antibodies for P-selectin (R&D Systems, clone AF737) were covalently conjugated to MPIOs in borate buffer with ammonium sulphate (pH 9.5), by incubation at 37°C for 48 h. The specificity of these MPIOs targeting P-selectin has been validated in a previous study.<sup>18</sup> MPIOs were then washed in phosphate buffered saline (PBS) containing 0.5% bovine serum albumin (BSA) at 4°C and incubated for 24 h at room temperature, to block the remaining active groups. MPIOs were rinsed in PBS (0.1% BSA) and stored at 4°C.

Imaging was carried out at Cyceron on a Pharmascan 7T/12 cm system using surface coils (Bruker) or at IRFMN on a 7T Bruker Biospec (Ettlingen, Germany) running ParaVision 6.01 and equipped with a quadrature cryogenic surface coil as transmitter and receiver. Three-dimensional

T2\*-weighted gradient echo imaging with flow compensation (GEFC) (spatial resolution of  $70 \times 70 \times 70 \mu\text{m}^3$ ), TE/TR 13.2 ms/200 ms and a flip angle (FA) of  $21^\circ$  was performed to visualize MPIOs. Specifications with the 7T Bruker Biospec system were the followings: resolution of  $80 \times 80 \times 80 \mu\text{m}^3$ , TE/TR = 7.5 ms/50 ms, FA of  $14^\circ$ . A baseline GEFC image was acquired before and after MPIO injection to evaluate the percentage of signal variation.

MRI acquisitions started immediately after the intravenous injection of MPIOs (200  $\mu\text{l}$  of 2 mg Fe/kg of conjugated MPIOs) and lasted 17–20 min. The quality of conjugated MPIOs was systematically checked in a mouse that received an intrastriatal injection of lipopolysaccharide (1  $\mu\text{l}$ , 1 mg/kg; coordinates: 0.5 mm anterior, 2.0 mm lateral, –3 mm ventral from the Bregma).

Furthermore, a high-resolution angiography was performed using a 3D-FLASH sequence suppressing signals from static tissue (Field of view (FOV) =  $30 \times 16 \times 8.4 \text{ mm}^3$ ; Resolution  $100 \times 100 \times 100 \mu\text{m}^3$ , FA of  $80^\circ$ ; TE/TR = 3.1 ms/16 ms; Number of average (NA) = 6; scan time: 16 min), only in mice subjected to the severe TBI model.

### [ $^3\text{H}$ ]DPA-714 autoradiography

Seven days ( $n = 7$  mice/group) or 21 days ( $n = 6$  mice/group) after mild TBI, brains were harvested, frozen in isopentane cooled at  $-35^\circ\text{C}$  and stored at  $-80^\circ\text{C}$ . Coronal brain sections 20- $\mu\text{m}$  thick (coordinates: Bregma –2.30 mm according to Franklin & Paxinos) were sliced using a cryostat at  $-20^\circ\text{C}$  (CM 3050S<sup>TM</sup>, Leica, Germany), collected on gelatin-coated slides and stored at  $-80^\circ\text{C}$  for at least 4 days. The density of TSPO binding sites was measured by *ex vivo* autoradiographic experiments using [ $^3\text{H}$ ]DPA-714 (Molar activity 2.01 GBq/ $\mu\text{mol}$ ).<sup>27,28</sup> Brain sections were allowed to equilibrate at room temperature (RT) for 3 hours and then incubated with 1 nmol/L of [ $^3\text{H}$ ]DPA-714 in 50 mmol/L Tris–HCl buffer pH 7.4 at RT for 60 minutes. The non-specific binding was measured in the presence of 1  $\mu\text{mol/L}$  PK-11195 (Sigma Aldrich, Lyon, France). Sections were rinsed twice in ice cold buffer ( $4^\circ\text{C}$ ) for 5 minutes, then briefly in distilled water at  $4^\circ\text{C}$  and dried at RT. Acquisitions were compiled over a period of 4 hours using the  $\beta$ -imager<sup>TM</sup> 2000 (Biospace Lab, Paris, France). Four sections were analyzed per mouse. ROIs were manually drawn on the ipsi- and contro-lateral hippocampus and frontal cortex. The level of bound radioactivity was directly determined by counting the number of  $\beta$ -particles emitted from the delineated area using the  $\beta$ -vision software (Biospace Lab, France). The radio-ligand signal in the ROIs was expressed as counts per

minute per square millimeter (cpm/ $\text{mm}^2$ ). Specific binding was determined by subtracting nonspecific binding from total binding.

### MicroPET experiments

PET experiments were conducted 21 days post mild TBI (5 mice). [ $^{18}\text{F}$ ]DPA-714 was prepared as described elsewhere<sup>29</sup> and obtained with a molar activity of 96 GBq/ $\mu\text{mol}$  at the time of injection. Mice were deeply anesthetized with isoflurane at 4–5% in  $\text{O}_2$  and maintained with 1.5–2% isoflurane during scanning. Mice were placed on a thermo-regulated bed (Minerve, France) in the prone position with a nose cone. Acquisitions were made on a microPET-CT SuperArgus system (Sedecal, Madrid, Spain) which has an effective axial/transaxial FOV of 4.8/6.7 cm, a spatial resolution less than 2 mm and a sensitivity above 2.5% in the whole FOV. Before PET acquisition, a 5-minute computed tomography (CT) scan was acquired for attenuation correction. [ $^{18}\text{F}$ ]DPA-714 was administered into the tail vein as a bolus ( $22 \pm 1 \text{ MBq}$ ). During the 50 minutes of PET acquisition, the respiratory rate and body temperature were monitored and kept as constant as possible.

The PET list-mode scans were rebinned into 27 frames: 4 frames of 10-seconds followed by 4 of 20-seconds, 4 of 60-seconds, 14 of 180-seconds, and 1 of 120-seconds. Each scan was corrected for randoms, scatter and attenuation, and the images were reconstructed using a 2D OSEM algorithm (GE Healthcare, France) into voxels of  $0.3875 \times 0.3875 \times 0.775 \text{ mm}^3$ . Dynamic PET images were corrected for partial volume effect using a Reblurred Van Cittert approach.<sup>30</sup> The estimation of the system point spread function (PSF) was slightly narrowed to avoid Gibbs ringing artifacts. Data summed over the entire acquisition were used for image registration. Since brain anatomy is very similar for mice of similar weight relatively to PET resolution, registration was accomplished as a rigid body transformation, with no warping or scaling. Each summed scan was individually smoothed with a Gaussian filter to improve the signal-to-noise ratio and to reduce the bias of misregistration into Mirrione template space. For this smoothing, a kernel of  $0.6 \times 0.6 \times 0.6 \text{ mm}^3$  FWHM was used. Each scan was coregistered using PMOD v3.4 software (PMOD Technologies Ltd, Switzerland) to a  $^{18}\text{F}$ FDG PET template in Mirrione coordinates using a mutual information similarity function with Powell's convergence optimization method.<sup>31</sup> The registered images were then used to create a template that was also registered to Mirrione space. Finally, all initial PET images were registered again to this template. The results were visually checked for misregistration.

To normalize the [ $^{18}\text{F}$ ]DPA-714 uptake, tissue activity was divided by the average whole brain activity. Each voxel of the 3D volume was paired with its corresponding contralateral voxel. Based on the Mirrione's template, regions of interest of at least 50 contiguous significant voxels were drawn from the z-score map using PMOD v3.2 software (PMOD Technologies Ltd, Switzerland). These regions of interest were then applied to individual [ $^{18}\text{F}$ ]DPA-714 images to retrieve [ $^{18}\text{F}$ ]DPA-714 uptake values in each brain.

### Immunohistochemistry

One, 7 or 21 days post-TBI, deeply anesthetized mice were transcardially perfused with cold heparinized saline (15 mL) and fixed with 100 mL of 2% paraformaldehyde and 0.2% picric acid phosphate buffer (pH 7.4) ( $n=4$  or 6 mice/group). Brains were post-fixed with 2% paraformaldehyde and 0.2% picric acid phosphate buffer (18 hours; 4°C) and cryoprotected (sucrose 20% in PBS; 24 hours; 4°C) before freezing in Tissue-Tek (Miles Scientific, Naperville, IL, USA). Cryostat-cut sections (10  $\mu\text{m}$ -thick sections) were collected on poly-lysine slides and stored at  $-80^\circ\text{C}$  before processing.

Sections were co-incubated overnight with rabbit polyclonal anti-mouse Iba1 (1:1000, Wako 019-19741), rat polyclonal anti-mouse CD68 (1:1000, Abcam 53444), goat polyclonal anti-mouse P-selectin (1:1000, RD System AF737), chicken polyclonal anti-mouse GFAP (1:2000, Abcam 4674), sheep anti-fibrinogen (1:10000, kind gift from Dr. E. Anglès Cano) and rabbit polyclonal anti-mouse Laminin (1:1500, Abcam 11575). Primary antibodies were revealed by using Fab'2 fragments of Donkey anti-rabbit linked to FITC or Cy5, anti-rat linked to Cy3, anti-goat IgG linked to FITC (1:600, Jackson ImmunoResearch, West Grove, USA). Infiltrated immunoglobulins were detected with a Cy3-conjugated Donkey Anti-Mouse IgG (1:600, Jackson ImmunoResearch 715-165-150). Washed sections were coverslipped with antifade medium containing DAPI. Epifluorescence images were digitally captured using a Leica DM6000 epifluorescence microscope-coupled coolsnap camera, visualized with Leica MM AF 2.2.0 software (Molecular Devices, USA) and further processed using ImageJ 1.52k software. Data collection and analyses were performed in a random order and blind to the experimental group, as well as to the ipsi/contralateral side. The quantifications were done in both ipsi- and contralateral cortices and hippocampi. A total of 15 to 18 images were quantified per animal. The number of astrocytes, microglia, activated microglia as well as infiltrated/perivascular macrophages were quantified in a total of 9 to 12 regions of interest,

divided in ipsi- versus contralateral sides of the TBI. We then compared the average number of cells between ipsi- and contralateral sides of the TBI. We also quantified the number of cells in sham animals that underwent all the surgical procedures but the TBI.

### Statistical analyses

Results are the mean  $\pm$  SD. For immunohistochemical analyses, cell counts were compared between ipsilateral versus contralateral regions of interest by the non-parametric Wilcoxon paired test. For cognitive functions (Y maze test and open field test), variables were compared by 2-way ANOVA followed by multiple comparisons with FDR corrections. For autoradiography, comparisons between the binding both sides were performed using the 2-way ANOVA and Bonferroni post-hoc test. The level of significance was  $p < 0.05$ . The intra-animal comparison of [ $^{18}\text{F}$ ]DPA-714 uptake between the ipsi- and contra-lateral sides in a brain area was performed using a Student *t*-test (normality was assessed using the Shapiro-Wilk test). For the *in vivo* microPET experiment, individual differences were calculated between paired voxels; 3D z-scores maps were calculated using a paired Wilcoxon non-parametric test. The statistical threshold was set at  $p < 0.01$ . All statistical tests were performed using GraphPad Prism software v9, San Diego, USA. All the experiments were done in a blind manner, and blinding was revealed after all analyses were processed.

## Results

### *Despite the lack apparent lesion on conventional MRI, a single mild TBI induces persistent behavioural deficits*

We first characterized our model of closed-head CCI to tailor the biomechanical injury to a degree not associated with brain damage on conventional MRI, thus mimicking one single mild TBI. Two depths of CCI (Figure 1(a)) were analyzed by MRI 24 h after TBI (Figure 1(b)). Impact immediately induced a respiratory arrest that was similar in both groups (Fig. S2,  $t = 33.18$  sec in miTBI;  $t = 57.27$  sec in modTBI,  $p = 0.1024$ ,  $n = 11$  mice/group). CCI at 1.5 mm depth did not induce any skull fracture and did not translate into measurable parenchymal lesion or bleeding on MRI (Figure 1(b)). By contrast, CCI at 2.0 mm depth led to a skull fracture, bleeding in the parenchyma in some animals, and to a 6  $\text{mm}^3$  edematous lesion ( $n = 7-8$  mice/group; Figure 1(b)). Based on these imaging findings, we thus selected CCI at 1.5 mm as a model of mild TBI (miTBI) and CCI at 2 mm as a model of moderate-to-severe TBI (modTBI).

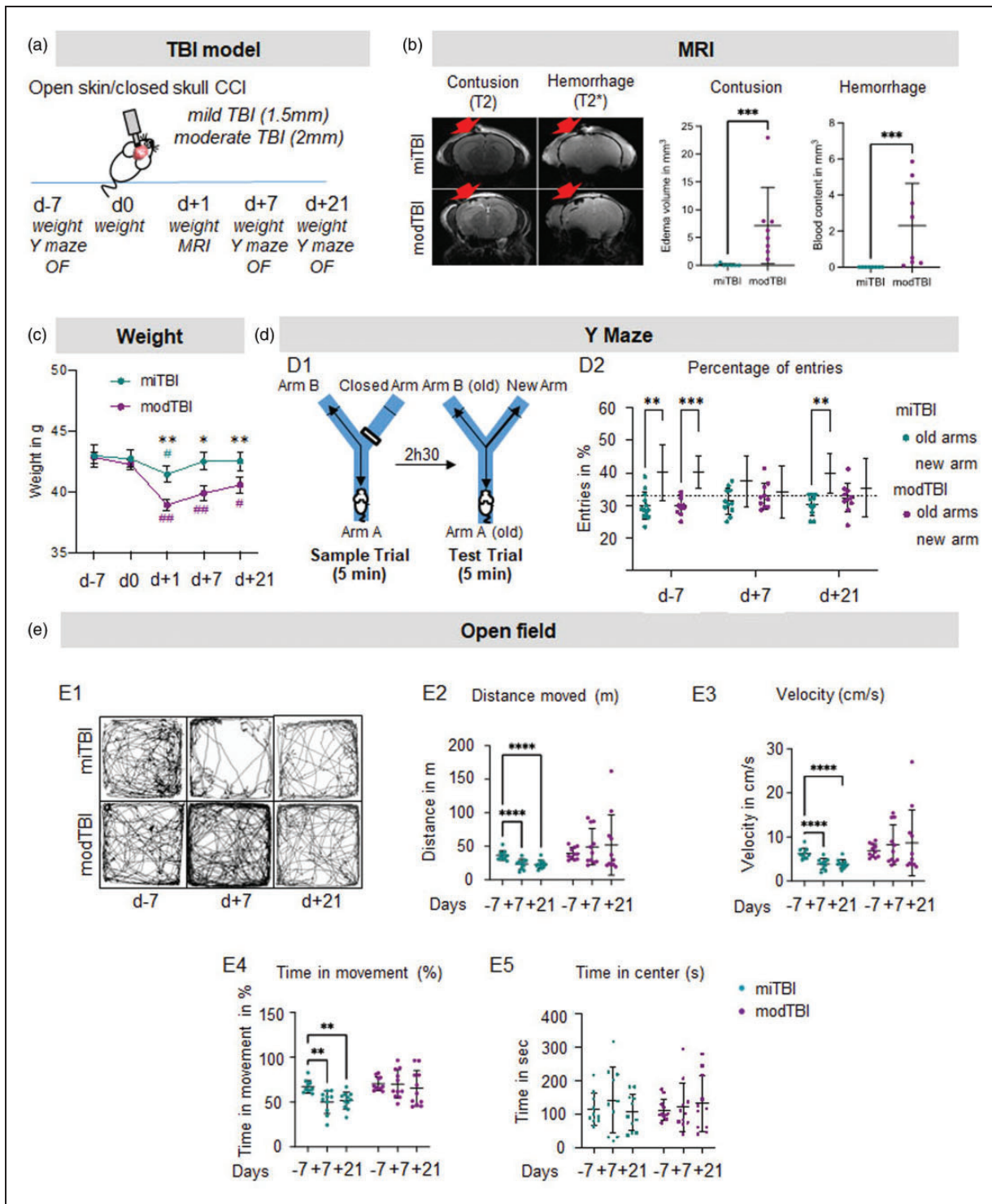


**Figure 1.** Mild TBI is undetectable by conventional MRI but induces long-term behavioural deficits. (a) Experimental design showing that two depths of impact (1.5 mm: mild TBI; 2 mm: moderate TBI) have been compared in the CCI model. (b) Representative T2-weighted (contusion) and T2\*-weighted (hemorrhage) MRI acquisitions and corresponding quantifications 24 hours after mild or moderate TBI.  $n = 7/8$  mice/group. \* $p < 0.05$  vs mild TBI; \*\* $p < 0.01$  vs mild TBI; \*\*\* $p < 0.001$  vs mild TBI, Mann-Whitney test; # $p < 0.05$  vs d0; ### $p < 0.01$  vs d0, Wilcoxon paired-test. Red arrows indicate the site of impact. (c) Measures of mouse weights 7 days before TBI, and day 0, 1, 7 and 21 days after TBI. (d) Schematic representation of Y maze behavioural test and quantifications of the percentage of entries in the new arm 7 days before and 7 and 21 days after mild or moderate TBI and (e) Representative sample traces and corresponding quantifications of the total distance moved, velocity, time of movement and time spend in the center on the open field test 7 days before, 7 and 21 days after mild or moderate TBI.  $n = 10$  mice/group, # $p < 0.05$  vs new arm, Wilcoxon paired-test; ### $p < 0.01$  vs d-7 Wilcoxon paired-test.

We then compared functional outcome after miTBI versus modTBI, as a function of time, before and after TBI. In both groups, mice lost weight 24 h after surgical procedure. Interestingly, miTBI mice recovered their weight at 7 days, while modTBI mice did not (Figure 1(c)). Four mice (out of 11) displayed circling episodes after modTBI (none in the miTBI group). These animals were not excluded from the study but contributed to the heterogeneity of the results. Spatial memory was evaluated using the Y maze 7 days before, then 7 and 21 days post-TBI (Figure 1(d1)). As expected, mice from both groups were initially able to differentiate the new arm from the old arms (number of entries >33.33%; Figure 1(d2)). However, mice were no longer able to discriminate old arms and the newly open arm 7 days after miTBI or modTBI (respectively  $p=0.30$  and  $p=0.75$  compared to 33.33%; Figure 1(d2)). Interestingly, this deficit was only transient in the miTBI group (38.2%,  $p=0.004$  compared to 33.33% at d+21) but not in the modTBI group (35.4%,  $p=0.32$  compared to 33.33% at d+21; Figure 1(d2)).

We also evaluated the general activity of mice using the open field test (Figure 1(e1)). We found an important decrease in the total distance ( $-36%$  d+7- and d+21 *vs* before surgery, Figure 1(e2)), the velocity ( $-37%$  d+7 and d+21 *vs* before surgery; Figure 1(e3)), and the time in movement ( $-26%$  and  $-28%$  d+7 and d+21 *vs* before surgery; Figure 1(e4)) in miTBI animals 7 and 21 days after miTBI. Velocity, distance and time in movement were significantly higher in modTBI animals versus miTBI animals. We did not detect any anxiety-like behaviour, since animals did not reduce their time spent in the center of the open field after surgery (Figure 1(e5)).

Altogether, these data highlighted that this mouse model of single miTBI induces persistent behavioural deficits without any evidence of a cerebral lesion on conventional imaging.

### Mild TBI does not induce cerebrovascular inflammation

In the absence of macroscopic lesion, we suspected that subtle cerebrovascular alterations may explain these behavioural deficits. In a previous study, we found in a mouse model of transient ischemic attack, that while conventional MRI detects no damage, molecular MRI, using MPIOs targeting the adhesion molecule P-selectin, allows a sensitive detection of an area of cerebrovascular inflammation.<sup>18</sup> We postulated that miTBI could as well induce an activation of the cerebral endothelium, and we thus transposed molecular imaging of P-selectin to our model, 1, 7 or 21 days post-miTBI (Figure 2). MPIOs coated with antibodies against

P-selectin were indeed able to bind the cerebral endothelium challenged by LPS-induced inflammation (Figure S3A for molecular MRI and S3B-C for immunohistochemistry). However, ultrasensitive MRI after administration of  $\alpha$ P-selectin MPIOs in miTBI mice did not detect any positive signal on MRI 1- (Figure 2(a) and (b);  $n=4$  mice/condition), 7- or 21-days post miTBI (Figure 2(a1);  $n=6$  mice/time). Sham animals and modTBI animals did not show any P-sel signals after 1 day (Figure 2(d)). The absence of P-selectin expression was confirmed by immunohistochemistry, with all six animals per group showing no signal at all (Figure 2(e);  $n=6$  mice/time). These data coincide with the absence of any leukocyte infiltration into the brain parenchyma after miTBI (data not shown). The lack of molecular MRI signal was not due to a failure of the technique: in a model of severe TBI (Figure S3D-H),  $\alpha$ P-selectin MPIOs induced a strong signal in the ipsilateral hemisphere (Figure 2(f)), which coincides with P-selectin expression by immunohistochemistry (Figure 2(g)). The specificity of the signal obtained by molecular MRI using MPIOs conjugated to P-selectin signal was confirmed by an absence of signal using MPIOs conjugated to isotypic immunoglobulins (IgG) (Figure S3H).

To assess blood-brain barrier (BBB) integrity, we performed stainings of fibrin/ogen and IgG. Although we could detect some positive signals for both fibrin/ogen and IgG in modTBI, we could not detect signals in miTBI (Figure S4), suggesting that the BBB integrity is unaffected by miTBI.

Altogether, these molecular MRI data show that in contrast to moderate-to-severe TBI, miTBI does not induce acute or delayed cerebrovascular inflammation.

### MicroPET imaging of TSPO unmask neuroinflammation after mild TBI

We then took advantage of the development of radio-labeled ligands of TSPO to investigate whether miTBI induces parenchymal neuroinflammation. First, *ex vivo* autoradiography was performed with [<sup>3</sup>H]DPA-714 (Figure 3(a1)). In the cortex, we observed a significantly higher specific binding of [<sup>3</sup>H]DPA-714 in the ipsi- *vs* contralateral cortex both at 7 days ( $8.90 \pm 1.00$  *vs*  $4.64 \pm 0.22$  cpm/mm<sup>2</sup>) and 21 days ( $8.73 \pm 0.57$  *vs*  $5.52 \pm 0.34$  cpm/mm<sup>2</sup>) after miTBI (Figure 3(a2)). In the hippocampus, a significantly higher specific binding of [<sup>3</sup>H]DPA-714 was measured in the ipsi- *vs* contralateral hemisphere both at 7 days ( $10.14 \pm 0.51$  *vs*  $6.14 \pm 0.32$  cpm/mm<sup>2</sup>) and 21 days ( $10.04 \pm 0.23$  *vs*  $6.78 \pm 0.25$  cpm/mm<sup>2</sup>) after miTBI (Figure 3(a3)).

These positive *ex vivo* autoradiography studies prompted us to explore TSPO imaging *in vivo* using the fluor-18 labeled analog of DPA-714. Analyses of

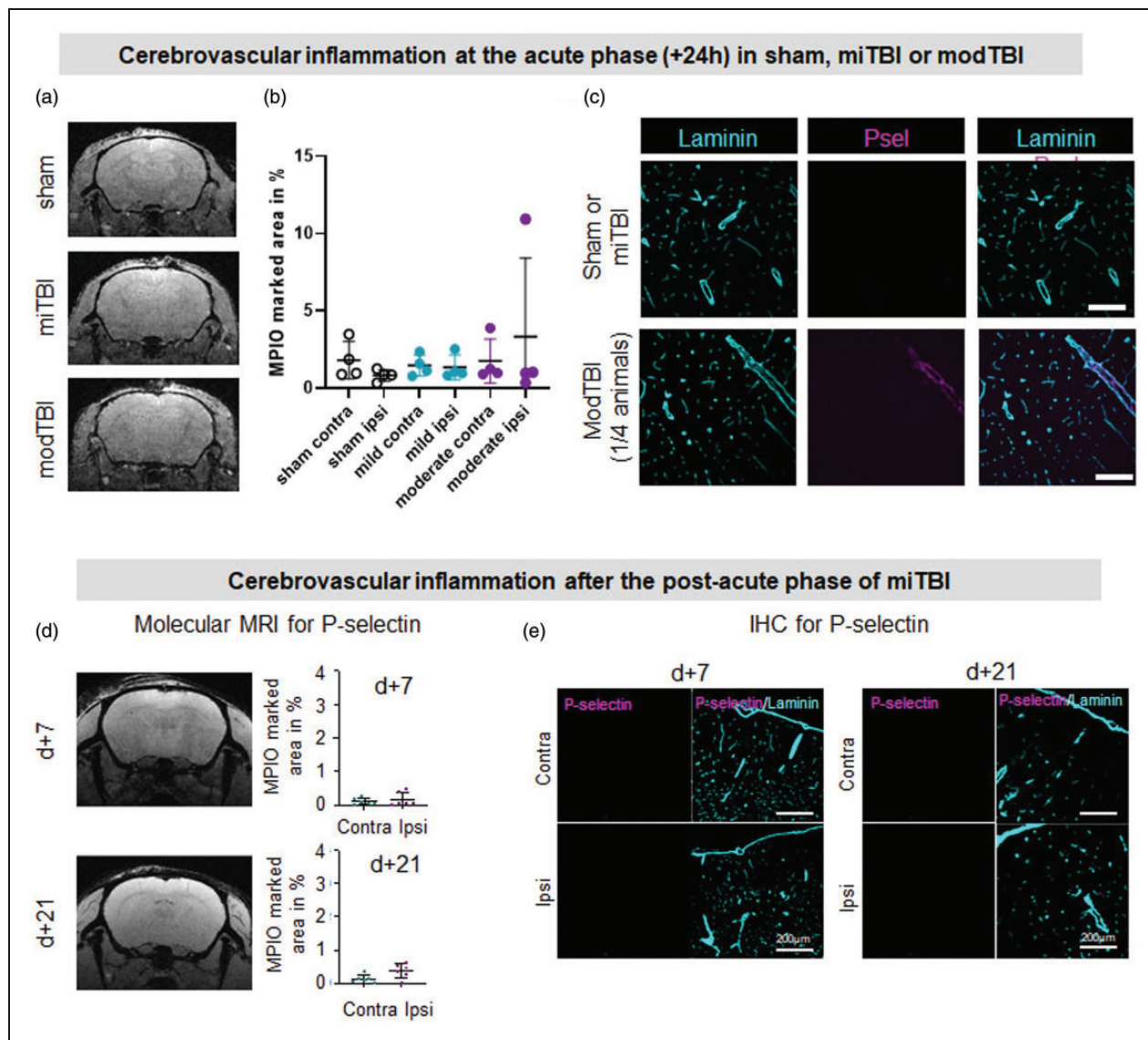


**Figure 2.** Unlike severe TBI, mild TBI does not induce cerebrovascular inflammation. (a, b) Representative T2\*-GEFC  $\alpha$ P-selectin MPIO acquisitions 24 h after sham surgery, miTBI or modTBI and their respective MPIO-marked area quantifications (n = 4 per condition). (c) Representative photomicrographs of P-selectin immunostaining 24 h after sham surgery, miTBI or modTBI (blood vessels were stained with laminin) (representative of 4 mice/group) (d) Representative T2\*-GEFC  $\alpha$ P-selectin MPIO acquisitions 7 and 21 days after miTBI and their respective MPIO-marked area quantifications and (e) Representative photomicrographs of P-selectin immunostaining 7 and 21 days after miTBI (blood vessels were stained with laminin) (n = 6 mice/group).

microPET acquisitions thus showed that the average images of [ $^{18}$ F]DPA-714 uptake detect an increased binding of the tracer in the cortex 21 days after miTBI (n = 5 mice/group; Figures 3(b1) and (b2)). The Z-score maps revealed a significant increased uptake of [ $^{18}$ F]DPA-714 in the ipsi- vs. contra-lateral cortex with a z-score value of  $6.05 \pm 1.86$  (Figure 3 (b3)). A small but significant increase in the ipsilateral uptake of [ $^{18}$ F]DPA-714 was also observed in a group of 50 voxels located in the hippocampus (z-score =  $5.74 \pm 1.32$ , Figure 3(b4)).

### *Mild TBI induces a long-lasting neuroinflammatory response in both ipsilateral cortex and hippocampus*

Since TSPO is generally considered as a marker of microglial/astroglial activation, we performed immunohistochemical analyses to support our PET findings. One day after miTBI, the number of microglial cells (Iba1+) tended to increase in the ipsilateral cortex (Figure S5A, +26% vs contralateral hemisphere), while the the number of activated microglial cells was already higher (Iba1+/CD68+) (Figure S5C, +1040%

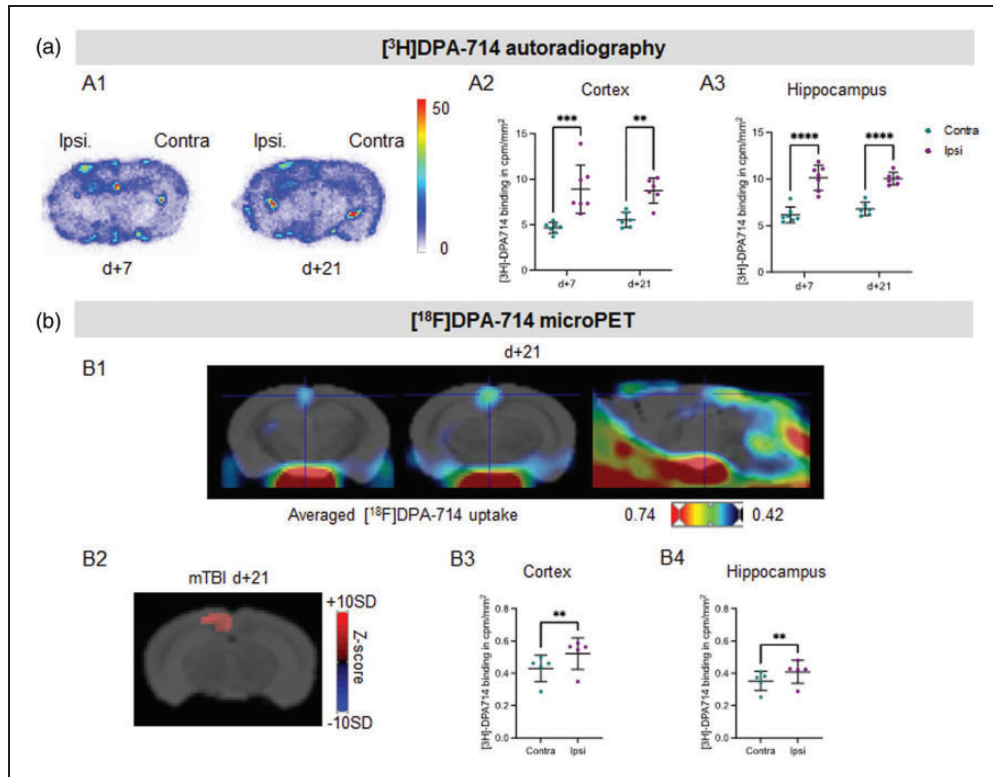


**Figure 3.** [<sup>3</sup>H]DPA-714 imaging reveals long-lasting neuroinflammation induced by mTBI. (a) *Ex vivo* autoradiographic experiment. (a1) Representative coronal brain sections of [<sup>3</sup>H]DPA-714 autoradiography 7 days and 21 days after mTBI. (a2) Quantifications of [<sup>3</sup>H]DPA-714 binding in cortex and hippocampus.  $n = 7$  mice/group,  $***p < 0.001$  vs contralateral ROI; 2-way ANOVA and (b) *In vivo* microPET experiment. (b1) Representative fusion images between a MRI template and images of averaged uptake of [<sup>18</sup>F]DPA-714 in 2 coronal images (left panels), and one sagittal image (right panel). (b2) Representative coronal brain image of Z-score maps fused with a MRI template showing [<sup>18</sup>F]DPA-714 uptake.  $n = 5$  mice,  $p < 0.01$  vs contralateral ROI. (b3,4) Quantifications of [<sup>18</sup>F]DPA-714 uptake in (b3) cortex and (b4) hippocampus 21 days after mTBI.  $n = 5$  mice,  $p = 0.0015$  vs contralateral cortex;  $p = 0.0022$  vs contralateral hippocampus.

vs contralateral hemisphere). The number of Iba1-/CD68+ cells near blood vessels, which we identified as infiltrated/perivascular macrophages began to increase (Figure S5B, +52% vs contralateral hemisphere). Microglial activation as well as the proportion of infiltrated/perivascular macrophages markedly increased at both 7- and 21 days after mTBI (7 days: Figure 4(a1), respectively; +774, +148, +233% vs contralateral hemisphere; 21 days: Figure 4(a2) and Figure S6A-3B, respectively; +219, +755 and +239% vs contralateral hemisphere).

Furthermore, microglial cell number also markedly increased 7 days after mTBI in the ipsilateral hippocampus (Figure 4(b1), +163% vs contralateral hemisphere), as well as activated microglia and infiltrated/perivascular macrophages (Figure S6C, respectively +379 and +230% vs contralateral hemisphere). This increase in microglial cell numbers persisted up to 21 days after mTBI but to a lesser degree than at 7 days (Figure 4(b2), +123% vs contralateral hemisphere), as well as activated microglia and infiltrated/perivascular

macrophages (Figure S6C, respectively +278 and +152% vs contralateral hemisphere).

We also performed immunohistochemical analyses 7- and 21-days post mTBI to assess astroglial activation as another index of neuroinflammation ( $n = 6$  mice/group). We found an increase in the number of cortical GFAP positive astrocytes 7 days after mTBI (Figure 4(c1); +385% vs contralateral hemisphere), which was even more pronounced 21 days after mTBI (Figure 4(c2); +1218% vs contralateral hemisphere). There was a notable astrocytic reactivity in the hippocampus 7 days after mTBI (see dotted areas in Figure 4(d1); +123% vs contralateral hemisphere). Hippocampal astrocyte numbers also increased 21 days after mTBI, but less than 7 days after mTBI (Figure 4(d2); +119% vs contralateral hemisphere).

Taken together, these data highlight that microPET was able to detect non-apparent lesions on MRI, which were correlated with persistent microglia/astrocyte activation in both the cortex and hippocampus.

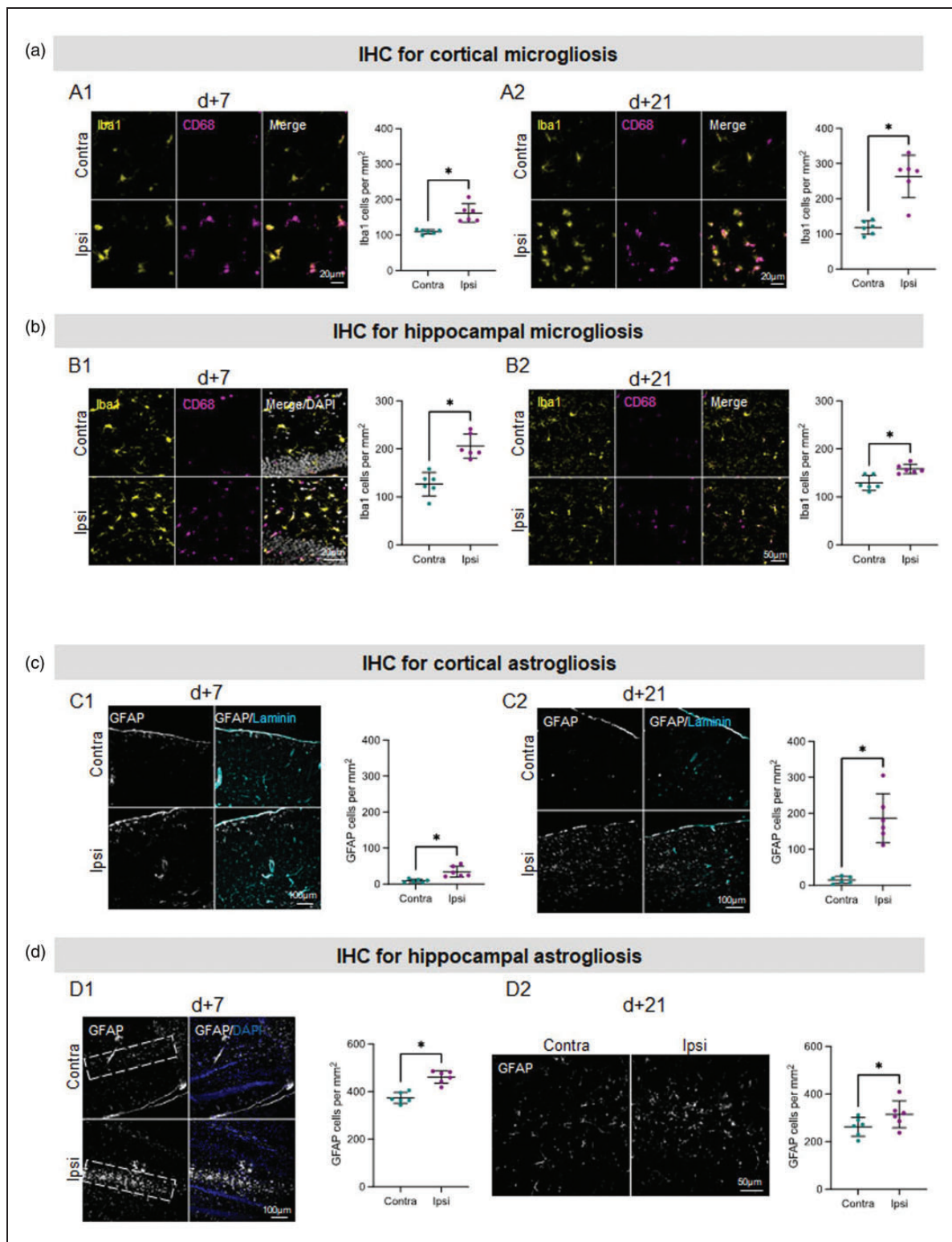


**Figure 4.** Immunohistochemistry analyses reveal long-lasting neuroinflammation induced by miTBI. (a and b) Long-lasting microglia induced by miTBI using Iba1 and CD68 immunostainings. (a) Cortical microglia. Representative photomicrographs of microglia and respective quantifications (a1) 7 days and (a2) 21 days after miTBI. (b) Hippocampal microglia. Representative photomicrographs of microglia and respective quantifications (b1) 7 days and (b2) 21 days after miTBI (c,d) Mild TBI provokes a long lasting astroglia. (a) GFAP positive astrocytes were found in the cortex 7 days after miTBI. (b) Astrocytes were found abundantly in the cortex 21 days after miTBI. (c) GFAP positive astrocytes were found abundantly in the hippocampus 7 days after miTBI. (d) Astrocytes were found in the hippocampus 21 days after miTBI.  $n = 6$  mice/group, \* $p < 0.05$ , \*\* $p < 0.01$  vs contralateral ROI, Wilcoxon paired-test.

## Discussion

The individual impact (severity of damages and cost) of patients with miTBI is lower than moderate to severe cases, but obviously, as a whole, this group of patients should not be neglected as they represent the largest contribution to the global burden of TBI<sup>1</sup>. For these patients, there is limited medical intervention for both diagnosis and acute therapy, and even less at the mid- and long-terms. However, a significant portion of miTBI patients suffers from persisting neurocognitive/psychological dysfunctions.<sup>1</sup> Furthermore, there is compelling evidence showing that patients suffering from repetitive miTBI (pediatric individuals, soldiers and sports players) develop brain abnormalities that likely explain long-term deficits.<sup>32</sup>

Here, we chose to investigate pathogenic mechanisms in a murine model of miTBI, the closed-head controlled cortical impact. This model has several advantages, including preservation of the skull and dura, and the fact that injury severity can be graded by adjusting impact depth and/or velocity.<sup>33</sup> Accordingly, we show that under a specific threshold of impact depth, conventional MRI detects neither contusion nor bleeding. Yet, animals in this case acutely lost weight, but more importantly, exhibited transient behavioural deficits in spatial memory and general activity that persist for at least after 21 days. These findings add to previous ones, that reported white and gray matter lesions associated with chronic behavioural deficits in mice subjected to opened-skull controlled cortical impact.<sup>34</sup> Collectively, these studies highlight the importance of considering patients with one single miTBI as patients with potential disabilities later in life. Risk-stratification by biomarker(s) may help predicting which patients with miTBI will develop cognitive/neurological dysfunctions.<sup>35</sup> Formerly, we developed a technique of molecular MRI targeting endothelial activation to uncover an area of inflammation in an experimental model of transient ischemic attack (another condition with no infarction on conventional imaging).<sup>18</sup> Using the same approach here, as well as a series of histological analyses, we detected cerebrovascular inflammation after moderate-to-severe TBI but not after miTBI. This indicates that therapeutic interventions focusing on cerebrovascular inflammation and leukocyte recruitment may be relevant to moderate-severe TBI,<sup>17,36</sup> but not to miTBI patients. By contrast, we found that one single miTBI induces a marked persistent parenchymal inflammatory response (microgliosis and astrogliosis), up to 3 weeks post injury, consistent with histological observations on human biopsies.<sup>37</sup> TBI has extensively been associated with microglial activation.<sup>38,39</sup> It also has been shown in another model of miTBI consisting on

compressing the thinned-skull bone, microglia can become activated.<sup>40</sup> Although one could argue that Iba1 is not a specific marker for microglial cells as it can also reflect infiltrating monocytes,<sup>38</sup> the absence of cerebrovascular inflammation in our model suggests that Iba1 staining mostly corresponds to microglia. Moreover, plasmatic levels of GFAP have been suggested to be a strong predictor/surrogate marker of miTBI severity, which also supports the idea that neuroinflammation is a key player after miTBI.<sup>41</sup> Considering its spatio-temporal profile, the neuroinflammatory response elicited in the present model of miTBI may participate in the functional deficits we observed, as previously shown in other mouse models of TBI.<sup>42–45</sup> Notably, the inflammatory response in our miTBI model occurred not only immediately underneath the biomechanical impact (i.e., at the cortical level), but also deeper in the brain, in the hippocampus, a structure well-known to control key memory processes. It would be very interesting to explore how manipulation of this inflammatory response could affect the persistent behavioural deficits. Indeed, anti-inflammatory treatments after TBI has shown some promising results, in both preclinical and clinical studies.<sup>46–48</sup>

Based on the higher frequency of TBI in men than in women, we performed our studies in male mice. It could be interesting to extend our work to females, as sex-related differences have been well documented in (neuro)inflammatory responses, including in intrinsic properties of microglial cells.<sup>49</sup>

Compared to fluid biomarkers, imaging biomarkers have the advantage to shed light on the brain pathogenic mechanisms recruited, and this at the spatial level. For instance, SPECT and PET studies have been performed to investigate regional perfusion and metabolic disturbances after miTBI.<sup>50</sup> TSPO imaging stands as an interesting approach, considering the great number of available radiotracers compatible with the clinical setting. With TSPO imaging, Coughlin and colleagues have provided alarming data showing that repetitive miTBI in NFL players induce a significant neuroinflammatory response, which may relate to brain dysfunctions.<sup>51</sup> Higher TSPO signals have also been reported even long after single events of moderate and severe TBI.<sup>13,52</sup> Finally, a recent study with the TSPO tracer [<sup>18</sup>F]PBR111 has suggested that combining PET and DTI could help predicting long term functional outcome after moderate TBI.<sup>53</sup> Altogether, these clinical observations pledge for the interest of TPSO imaging, but to our knowledge, no data is yet available for patients after a single mild TBI.

TSPO imaging in experimental models has largely confirmed the occurrence of an extensive neuroinflammatory response after moderate or severe TBI.<sup>54–58</sup>

Regarding miTBI, a previous microPET study did not report a higher brain uptake of [ $^{18}\text{F}$ ]DPA-714<sup>58</sup>. By contrast, we were able to detect a long-lasting increased signal in the ipsilateral hemisphere in our closed-head mild TBI model, both *ex vivo* (autoradiography with [ $^3\text{H}$ ]DPA-714) and *in vivo* (microPET with [ $^{18}\text{F}$ ]DPA-714). Thanks to its higher resolution compared to microPET, autoradiography suggested the occurrence of neuroinflammation both at the cortical and hippocampal levels. This was further supported by our immunostainings, reporting a strong and persisting microglial activation in the cortex and hippocampus. While microglia, astrocytes and endothelial cells may all be able to produce TSPO,<sup>59</sup> our immunohistochemical and molecular imaging analyses suggest that the PET signals we observed originated from glial, but not endothelial responses.

In conclusion, we provide a solid proof of concept that one single mild TBI can induce long-lasting behavioural deficits, as well as a neuroinflammatory response, despite no lesion detectable by conventional imaging techniques. As revealed by our microPET study, we propose that patients with miTBI and persistent cognitive abnormalities could suffer from neuroinflammatory responses, possibly at the origin of functional sequelae.

## Abbreviations

CCI: controlled cortical impact; CSF: cerebrospinal fluid; GFAP: glial fibrillary acid protein; Iba1: Iodinated calcium-binding adapter molecule-1; LPS: lipopolysaccharide; MPIO: Microparticle of iron oxide; MRI: magnetic resonance imaging; MSME: multi-spin multi-echo; miTBI: mild traumatic brain injury; PET: positron emission tomography; SPECT: single photon emission computed tomography; TBI: traumatic brain injury; TSPO: translocator protein; USPIO: ultra-small particles of iron oxide; VCAM-1: vascular cell adhesion molecule-1

## Funding

The author(s) disclosed receipt of the following financial support for the research, authorship, and/or publication of this article: This work was supported by Institut National de la Santé Et de la Recherche Médicale (INSERM), Caen Normandy University (UNICAEN), Institut pour la Recherche sur la Moelle épinière et l'Encéphale (IRME), Union Nationale des Associations de Familles de Traumatismes crâniens et de Cérébro-lésés (UNAFTC), and by Labex IRON (ANR-11-LABX-18-01).

## Acknowledgements

We are grateful to Julie Busson for technical assistance.

## Declaration of conflicting interests

The author(s) declared no potential conflicts of interest with respect to the research, authorship, and/or publication of this article.

## Authors' contributions

Designed the study (AD, SC, DV, CA), performed experiments (AD, AL, PP, ZG, SP, GV, DT, SS, JV, DL, BK, CA), analysed data (AD, AL, ZG, GV, SS, LG, CT, EZ), drafted the manuscript (AD, AL, LG, MR, EZ, SC, DV, CA).

## ORCID iD

Damien Levard  <https://orcid.org/0000-0002-7275-3170>

## Supplemental material

Supplemental material for this article is available online.

## References

1. Maas AIR, Menon DK, Adelson PD, et al. Traumatic brain injury: integrated approaches to improve prevention, clinical care, and research. *Lancet Neurol* 2017; 16: 987–1048.
2. Dewan MC, Rattani A, Gupta S, et al. Estimating the global incidence of traumatic brain injury. *J Neurosurg* 2019; 130: 1080–1097.
3. Teasdale G and Jennett B. Assessment of coma and impaired consciousness: a practical scale. *The Lancet* 1974; 304: 81–84.
4. Cruz-Haces M, Tang J, Acosta G, et al. Pathological correlations between traumatic brain injury and chronic neurodegenerative diseases. *Transl Neurodegener* 2017; 6: 20.
5. Gardner RC and Yaffe K. Epidemiology of mild traumatic brain injury and neurodegenerative disease. *Mol Cell Neurosci* 2015; 66: 75–80.
6. Perry DC, Sturm VE, Peterson MJ, et al. Association of traumatic brain injury with subsequent neurological and psychiatric disease: a meta-analysis. *JNS* 2016; 124: 511–526.
7. Madsen T, Erlangsen A, Orlovskaya S, et al. Association between traumatic brain injury and risk of suicide. *JAMA* 2018; 320: 580–588.
8. Stein MB, Jain S, Giacino JT, et al. Risk of posttraumatic stress disorder and major depression in civilian patients after mild traumatic brain injury: a TRACK-TBI study. *JAMA Psychiatry* 2019; 76: 249–258.
9. Jassam YN, Izzy S, Whalen M, et al. Neuroimmunology of traumatic brain injury: time for a paradigm shift. *Neuron* 2017; 95: 1246–1265.
10. Zinnhardt B, Wiesmann M, Honold L, et al. In vivo imaging biomarkers of neuroinflammation in the development and assessment of stroke therapies – towards clinical translation. *Theranostics* 2018; 8: 2603–2620.
11. Dani M, Wood M, Mizoguchi R, et al. Microglial activation correlates in vivo with both tau and amyloid in Alzheimer's disease. *Brain* 2018; 141: 2740–2754.

12. Hagens MH, Killestein J, Yaqub MM, et al. Cerebral rituximab uptake in multiple sclerosis: a <sup>89</sup>Zr-immunoPET pilot study. *Mult Scler* 2018; 24: 543–545.
13. Ramlackhansingh AF, Brooks DJ, Greenwood RJ, et al. Inflammation after trauma: microglial activation and traumatic brain injury. *Ann Neurol* 2011; 70: 374–383.
14. Gauberti M, Fournier AP, Docagne F, et al. Molecular magnetic resonance imaging of endothelial activation in the central nervous system. *Theranostics* 2018; 8: 1195–1212.
15. Fournier AP, Quenault A, Lizarrondo SM, et al. Prediction of disease activity in models of multiple sclerosis by molecular magnetic resonance imaging of P-selectin. *Proc Natl Acad Sci U S A* 2017; 114: 6116–6121.
16. Gauberti M, Montagne A, Marcos-Contreras OA, et al. Ultra-sensitive molecular MRI of vascular cell adhesion molecule-1 reveals a dynamic inflammatory penumbra after strokes. *Stroke* 2013; 44: 1988–1996.
17. Vegliante G, Tolomeo D, Drieu A, et al. Longitudinal molecular magnetic resonance imaging of endothelial activation after severe traumatic brain injury. *JCM* 2019; 8: 1134.
18. Quenault A, Martinez de Lizarrondo S, Etard O, et al. Molecular magnetic resonance imaging discloses endothelial activation after transient ischaemic attack. *Brain* 2017; 140: 146–157.
19. Percie Du Sert N, Hurst V, Ahluwalia A, et al. The ARRIVE guidelines 2.0: updated guidelines for reporting animal research. *J Cereb Blood Flow Metab* 2020; 40: 1769–1777.
20. Brody DL, Mac Donald C, Kessens CC, et al. Electromagnetic controlled cortical impact device for precise, graded experimental traumatic brain injury. *J Neurotrauma* 2007; 24: 657–673.
21. Zanier ER, Bertani I, Sammal E, et al. Induction of a transmissible tau pathology by traumatic brain injury. *Brain* 2018; 141: 2685–2699.
22. Toyama K, Spin JM, Abe Y, et al. Controlled isoflurane anesthesia exposure is required for reliable behavioral testing in murine surgical models. *J Pharmacol Sci* 2019; 140: 106–108.
23. Yasko JR, Moss IL and Mains RE. Transcriptional profiling of non-injured nociceptors after spinal cord injury reveals diverse molecular changes. *Front Mol Neurosci* 2019; 12: 284.
24. Obiang P, Macrez R, Jullienne A, et al. GluN2D subunit-containing NMDA receptors control tissue plasminogen activator-mediated spatial memory. *J Neurosci* 2012; 32: 12726–12734.
25. Pruvost M, Lépine M, Leonetti C, et al. ADAMTS-4 in oligodendrocytes contributes to myelination with an impact on motor function. *Glia* 2017; 65: 1961–1975.
26. Prut L and Belzung C. The open field as a paradigm to measure the effects of drugs on anxiety-like behaviors: a review. *Eur J Pharmacol* 2003; 463: 3–33.
27. Damont A, Garcia-Argote S, Buisson DA, et al. Efficient tritiation of the translocator protein (18 kDa) selective ligand DPA-714. *J Labelled Comp Radiopharm* 2015; 58: 1–6.
28. Foucault-Fruchard L, Doméné A, Page G, et al. Neuroprotective effect of the alpha 7 nicotinic receptor agonist PHA 543613 in an in vivo excitotoxic adult rat model. *Neuroscience* 2017; 356: 52–63.
29. Sérrière S, Tauber C, Vercoillie J, et al. Amyloid load and translocator protein 18 kDa in APP<sup>swe</sup>PS1-dE9 mice: a longitudinal study. *Neurobiol Aging* 2015; 36: 1639–1652.
30. Carasso AS. Linear and nonlinear image deblurring: a documented study. *SIAM J Numer Anal* 1999; 36: 1659–1689.
31. Mirrione MM, Schiffer WK, Fowler JS, et al. A novel approach for imaging brain-behavior relationships in mice reveals unexpected metabolic patterns during seizures in the absence of tissue plasminogen activator. *NeuroImage* 2007; 38: 34–42.
32. Fehily B and Fitzgerald M. Repeated mild traumatic brain injury: potential mechanisms of damage. *Cell Transplant* 2017; 26: 1131–1155.
33. Ren Z, Iliff JJ, Yang L, et al. ‘Hit & run’ model of closed-skull traumatic brain injury (TBI) reveals complex patterns of post-traumatic AQP4 dysregulation. *J Cereb Blood Flow Metab* 2013; 33: 834–845.
34. Leconte C, Benedetto C, Lentini F, et al. Histological and behavioral evaluation after traumatic brain injury in mice: a ten months follow-up study. *J Neurotrauma* 2020; 37: 1342–1357.
35. Sharma R, Rosenberg A, Bennett ER, et al. A blood-based biomarker panel to risk-stratify mild traumatic brain injury. *Plos ONE* 2017; 12: e0173798.
36. Needham EJ, Helmy A, Zanier ER, et al. The immunological response to traumatic brain injury. *J Neuroimmunol* 2019; 332: 112–125.
37. Engel S, Schluesener H, Mittelbronn M, et al. Dynamics of microglial activation after human traumatic brain injury are revealed by delayed expression of macrophage-related proteins MRP8 and MRP14. *Acta Neuropathol* 2000; 100: 313–322.
38. Willis EF, MacDonald KPA, Nguyen QH, et al. Repopulating microglia promote brain repair in an IL-6-dependent manner. *Cell* 2020; 180: 833–846.e16.
39. Witcher KG, Bray CE, Chunchai T, et al. Traumatic brain injury causes chronic cortical inflammation and neuronal dysfunction mediated by microglia. *J Neurosci* 2021; 41: 1597–1616.
40. Roth TL, Nayak D, Atanasijevic T, et al. Transcranial amelioration of inflammation and cell death after brain injury. *Nature* 2014; 505: 223–228.
41. Gill J, Latour L, Diaz-Arrastia R, et al. Glial fibrillary acidic protein elevations relate to neuroimaging abnormalities after mild TBI. *Neurology* 2018; 91: e1385–e1389.
42. Caplan HW, Cardenas F, Gudenkauf F, et al. Spatiotemporal distribution of microglia after traumatic brain injury in male mice. *ASN Neuro* 2020; 12: 1759091420911770.
43. Henry RJ, Ritzel RM, Barrett JP, et al. Microglial depletion with CSF1R inhibitor during chronic phase of experimental traumatic brain injury reduces neurodegeneration and neurological deficits. *J Neurosci* 2020; 40: 2960–2974.

44. Loane DJ and Kumar A. Microglia in the TBI brain: the good, the bad, and the dysregulated. *Exp Neurol* 2016; 275 Pt 3: 316–327.
45. Toledano Furman N, Gottlieb A, Prabhakara KS, et al. High-resolution and differential analysis of rat microglial markers in traumatic brain injury: conventional flow cytometric and bioinformatics analysis. *Sci Rep* 2020; 10: 11991.
46. Bergold PJ. Treatment of traumatic brain injury with anti-inflammatory drugs. *Exp Neurol* 2016; 275 Pt 3: 367–380.
47. Xu X, Gao W, Cheng S, et al. Anti-inflammatory and immunomodulatory mechanisms of atorvastatin in a murine model of traumatic brain injury. *J Neuroinflammation* 2017; 14: 167.
48. Begemann M, Leon M, van der Horn HJ, et al. Drugs with anti-inflammatory effects to improve outcome of traumatic brain injury: a meta-analysis. *Sci Rep* 2020; 10: 16179.
49. Lynch MA. Exploring sex-related differences in microglia may be a game-changer in precision medicine. *Front Aging Neurosci* 2022; 14: 868448.
50. Raji CA and Henderson TA. PET and single-photon emission computed tomography in brain concussion. *Neuroimaging Clin N Am* 2018; 28: 67–82.
51. Coughlin JM, Wang Y, Munro CA, et al. Neuroinflammation and brain atrophy in former NFL players: an in vivo multimodal imaging pilot study. *Neurobiol Dis* 2015; 74: 58–65.
52. Folkersma H, Boellaard R, Yaqub M, et al. Widespread and prolonged increase in (R)-11C-PK11195 binding after traumatic brain injury. *J Nucl Med* 2011; 52: 1235–1239.
53. Missault S, Anckaerts C, Blockx I, et al. Neuroimaging of subacute brain inflammation and microstructural changes predicts long-term functional outcome after experimental traumatic brain injury. *J Neurotrauma* 2019; 36: 768–788.
54. Venneti S, Wagner AK, Wang G, et al. The high affinity peripheral benzodiazepine receptor ligand DAA1106 binds specifically to microglia in a rat model of traumatic brain injury: Implications for PET imaging. *Exp Neurol* 2007; 207: 118–127.
55. Cao T, Thomas TC, Ziebell JM, et al. Morphological and genetic activation of microglia after diffuse traumatic brain injury in the rat. *Neuroscience* 2012; 225: 65–75.
56. Grossman R, Paden CM, Fry PA, et al. Persistent region-dependent neuroinflammation, NMDA receptor loss and atrophy in an animal model of penetrating brain injury. *Future Neurol* 2012; 7: 329–339.
57. Donat CK, Gaber K, Meixensberger J, et al. Changes in binding of [123I]CLINDE, a High-Affinity translocator protein 18 kDa (TSPO) selective radioligand in a rat model of traumatic brain injury. *Neuromolecular Med* 2016; 18: 158–169.
58. Israel I, Ohsiek A, Al-Momani E, et al. Combined [18F] DPA-714 micro-positron emission tomography and autoradiography imaging of microglia activation after closed head injury in mice. *J Neuroinflammation* 2016; 13: 140.
59. Guilarte TR. TSPO in diverse CNS pathologies and psychiatric disease: a critical review and a way forward. *Pharmacol Ther* 2019; 194: 44–58.